Catalysis Today 154 (2010) 133–141

Contents lists available at ScienceDirect

Catalysis Today

journal homepage: www.elsevier.com/locate/cattod

Exhaust gas recirculation for on-board hydrogen production by isooctane reforming: Comparison of performances of metal/ceria–zirconia based catalysts prepared through pseudo sol–gel or impregnation methods

Emmanuelle Ambroise [a], Claire Courson [a], Anne-Cécile Roger [a], Alain Kiennemann [a,*], Gilbert Blanchard [b], Séverine Rousseau [b], Xavier Carrier [c], Eric Marceau [c], Camille La Fontaine [d], Françoise Villain [d]

[a] Laboratoire des Matériaux, Surfaces et Procédés pour la Catalyse (UMR 7515 CNRS), Université de Strasbourg, 25 rue Becquerel, 67087 Strasbourg, France
[b] PSA Peugeot Citroën - Centre Technique de VELIZY - Sciences et Technologies Emergentes pour le Post traitement - Science pour l'Automobile et Recherche Avancée, 78943 Vélizy-Villacoublay, France
[c] Laboratoire de Réactivité de Surface (UMR 7197 CNRS), UPMC (Université Pierre et Marie Curie - Paris 6), 4 place Jussieu, 75252 Paris Cedex 05, France
[d] Synchrotron SOLEIL, L'Orme des Merisiers, BP48, Saint-Aubin, 91192 Gif-sur Yvette, France

ARTICLE INFO

Article history:
Available online 15 January 2010

Keywords:
Hydrogen
EGR
Reforming
Ceria–zirconia

ABSTRACT

Isooctane reforming under conditions which are set by exhaust gas can be used to generate hydrogen on-board. Isooctane reforming reactivity tests have been performed with bimetallic catalysts Co-noble metal/ceria–zirconia, prepared either by insertion of transition metal in a ceria–zirconia matrix, either by their impregnation on ceria–zirconia. The influence of the preparation procedure on the activity of the noble metal-doped catalysts is discussed.

1. Introduction

Stringent European directives on reducing pollutant emissions from fossil fuel-based engines require that the emission of nitrogen oxides (NO_x) be strictly limited. This has motivated car manufacturers to develop post-treatment systems as deNO_x in three-way catalysts (TWC) [1], selective catalytic reduction (SCR) of NO_x by hydrocarbons [2] or by hydrogen [3], or NO_x-Trap [4].

Exhaust gas recirculation (EGR) system can also be an effective technique involved in reducing NO_x emissions [5–9]. This system is based on the principle of recirculating the exhaust gases through a control valve back into the inlet manifold where they mix with the fresh air and get diluted with the intake charge. Recirculated gases thus behave as an additional diluent in the unburned gas mixture and reduce the flame temperature and the oxygen concentration in the combustion chamber, leading to decrease NO formation rates [10]. This system has been used mainly in Diesel engines since the early 1970s to lower fuel consumption and pollutant exhaust contents as NO_x and unburned hydrocarbons [5,11]. However, applying EGR to a Diesel engine leads to increasing the production of particulate matter [12]. To decrease NO_x emissions in an environmentally friendly way, Diesel vehicles should be also equipped with a particulate filter and a fuel-borne cerium catalyst [13].

Since hydrogen is one of the best fuels to be used in internal combustion (IC) engines in addition to conventional hydrocarbons, and particularly to gasoline [14], the EGR system could be beneficially used also to generate hydrogen on-board, by catalytic reforming of co-fed fuel by exhaust gases (see Fig. 1), leading to improvements in terms of brake power, thermal efficiency, combustion robustness and reduction of HC, CO, CO_2, and NO_x emissions [15–17]. Reformed EGR (REGR) creates a gradual bridge towards hydrogen-fuelled car, without radical change of the existing motorizations.

The present study focuses on catalytic isooctane reforming, a gasoline surrogate, assuming there is not a significant effect of sulphur-containing fuels on catalytic reforming [18].

Reforming has been performed under conditions which are set by and are directly linked to the internal combustion engine operation. The purpose of this work is to recirculate, after reforming, an effluent containing 10–15% of hydrogen into the combustion chamber, so that an equivalent efficiency of the engine can be maintained.

The largest part of studies dealing with hydrocarbon reforming has been conducted with transition metals supported on oxides.

* Corresponding author. Tel.: +33 3 68 85 27 66; fax: +33 3 68 85 27 68.
E-mail addresses: kiennemann@unistra.fr, Kiennemann@chimie.u-strasbg.fr (A. Kiennemann).

0920-5861/$ – see front matter © 2010 Elsevier B.V. All rights reserved.
doi:10.1016/j.cattod.2009.12.010

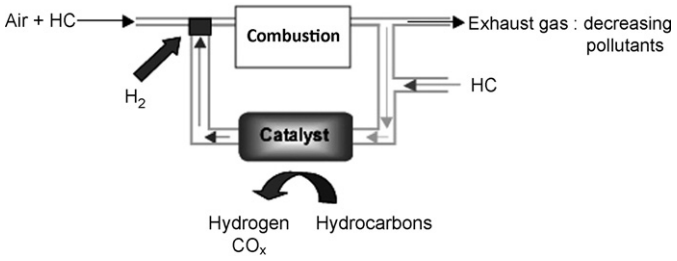

Fig. 1. Schematic diagram of REGR system.

In contrast, our innovative approach to a catalytic system consists of the active phase integration into a support with high oxygen mobility [19], which would enhance the metal-support interaction, consequently decrease the formation of carbonaceous deposits and prevent loss of toxic metal (as cobalt) during reaction. Accordingly, bimetallic Co–Rh catalysts prepared by precursor method, which allows insertion of metallic cation in ceria–zirconia matrix, have been chosen for hydrocarbon reforming reaction and have proven to be efficient for hydrogen production [20,21].

In the present study, textural, structural, redox properties and catalytic activity of ceria–zirconia based Co–Rh catalysts, prepared via impregnation or by precursor method (sol–gel route) will be compared. Special attention has been paid to characterization by XRD, TPR and XANES in order to assess the integration of cobalt in the catalysts. The influence of the ceria content on the catalytic activity will also be evaluated.

2. Experimental

2.1. Catalysts preparation

Two series of catalysts were prepared by sol–gel and impregnation methods respectively. In each series, the chemical compositions were based both on a stoichiometric ceria–zirconia (ceria: 58 wt.%, zirconia: 42 wt.%) and on a ceria-rich ceria–zirconia (ceria: 80 wt.%, zirconia: 20 wt.%). Cobalt based catalysts contained 5 wt.% of cobalt. Co–Rh bimetallic catalysts contained a variable amount of rhodium (0.5 or 1.0 wt.%) and an amount of cobalt lower than 5 wt.%, so that the molar amount in metals was kept constant.

Sol–gel catalysts were synthesized by a pseudo sol–gel method, based on the thermal decomposition of propionate precursors [19]. The appropriate starting salts were all dissolved in hot propionic acid for a cation concentration of 0.12 mol L^{-1}. The starting salts for Ce, Zr, Co and Rh were cerium(III) acetate hydrate, zirconium(IV) acetylacetonate, cobalt(II) acetate hydrate, rhodium(II) acetate dimer, which led exclusively to propionate precursors in propionic acid. The hot solutions were mixed and boiled for 1 h before the solvent was evaporated until a resin was obtained. This resin was heated at 2 °C min^{-1} in air until 500 °C and maintained 6 h at this temperature. The catalytic materials prepared via a sol–gel route are referred to as CZ^S.

Impregnated catalysts were prepared by wet impregnation on ceria–zirconias supplied by Rhodia Electronics & Catalysis. The cobalt precursor (cobalt(II) acetate hydrate) was dissolved in a volume of water corresponding to the porous volume of the support. The support was added to the aqueous solution and the mixture was left in moist atmosphere during 1 h for maturation. The metal-supported oxide was then dried at 120 °C for 2 h, and calcined from room temperature to 500 °C at a rate of 2 °C min^{-1}, followed by a 2 h plateau at that temperature.

For Co–Rh bimetallic catalysts, rhodium (rhodium(III) nitrate) was added by impregnation to a formerly calcined cobalt-containing catalyst. The supports supplied by Rhodia and the catalytic materials prepared by impregnation are referred to as CZ^R.

The formulations of the catalysts are summarized in Table 1. The experimental content (e.a.) in metals (Co, Rh) was determined by ICP (inductively coupled plasma) at the Vernaison Center for Chemical Analysis of the CNRS. For both sol–gel and impregnated catalysts, cobalt and rhodium contents are very close to the theoretical values (th.).

2.2. Catalysts characterization

Specific surface areas were determined by nitrogen physisorption measurements at 77 K (Brunauer–Emmett–Teller, BET method) using a COULTER SA 3100. Prior to the analysis, the samples were outgassed at 250 °C for 16 h.

The structure of the mixed oxides was examined by X-ray diffraction (XRD) on a BRUKER D8 Advance using Cu Kα radiation (λ = 1.5418 Å). The intensity data were collected over a 2θ range of 20–100° with a step size of 0.008° and a count time of 4 s per step. The $K\alpha_2$ contribution was eliminated from the diffraction by computer post-processing. The lattice parameters (a) of the samples have been calculated by Eq. (1), characteristic of cubic phase, with d: the interreticular distance, and hkl the Miller indexes. The particle sizes (D) have been determined by Debye–Scherrer equation, from X-ray line width broadening, taken

Table 1
Composition of prepared catalysts.

Catalyst code	Theoretical formulation	Composition (wt.%)					
		Ce (th.)	Zr (th.)	Co (th.)	Co (e.a.)	Rh (th.)	Rh (e.a.)
CZ^S(58-42)	$Ce_2Zr_2O_8$	47.4	30.9	–	–	–	–
CZ^S(58-42)Co	$Ce_{1.75}Zr_{1.75}Co_{0.50}O_8$	43.7	28.4	5.1	5.08	–	–
CZ^S(58-42)Co–Rh(0.5)	$Ce_{1.75}Zr_{1.75}Co_{0.47}Rh_{0.03}O_8$	43.6	28.4	4.8	4.56	0.5	0.45
CZ^R(58-42)	$Ce_2Zr_2O_8$	47.4	30.9	–	–	–	–
CZ^R(58-42) + Co	$Co/Ce_2Zr_2O_8$	43.7	28.4	5.1	4.80	–	–
CZ^R(58-42) + Co + Rh(0.5)	$Co + Rh/Ce_2Zr_2O_8$	43.6	28.4	4.8	4.90	0.5	0.61
CZ^S(80-20)	$Ce_{2.96}Zr_{1.04}O_8$	65.1	14.8	–	–	–	–
CZ^S(80-20)Co	$Ce_{2.60}Zr_{0.91}Co_{0.49}O_8$	60.3	13.7	4.8	4.64	–	–
CZ^S(80-20)Co–Rh(0.5)	$Ce_{2.58}Zr_{0.90}Co_{0.49}Rh_{0.03}O_8$	59.9	13.6	4.8	4.64	0.5	0.43
CZ^S(80-20)Co–Rh(1.0)	$Ce_{2.57}Zr_{0.90}Co_{0.46}Rh_{0.07}O_8$	59.6	13.6	4.5	4.29	1.0	0.70
CZ^R(80-20)	$Ce_{2.96}Zr_{1.04}O_8$	65.1	14.8	–	–	–	–
CZ^R(80-20) + Co	$Co/Ce_{2.96}Zr_{1.04}O_8$	60.3	13.7	4.8	4.30	–	–
CZ^R(80-20) + Co + Rh(0.5)	$Co + Rh/Ce_{2.96}Zr_{1.04}O_8$	59.9	13.6	4.8	4.32	0.5	0.62
CZ^R(80-20) + Co + Rh(1.0)	$Co + Rh/Ce_{2.96}Zr_{1.04}O_8$	59.6	13.6	4.5		1.0	

Table 2
Textural and structural characteristics of prepared catalysts.

Catalyst code	Lattice parameter, a (Å)	Mixed oxide particle size, D (nm)	Co_3O_4 particle size, D Co_3O_4 (nm)	BET SSA ($m^2\,g^{-1}$)
CZ^S(58-42)	5.29	4.4	–	64
CZ^S(58-42)Co	5.27	3.9	8.9	72
CZ^S(58-42)Co–Rh(0.5)	5.27	3.8	5.0	75
CZ^R(58-42)	5.28	6.4	–	101
CZ^R(58-42) + Co	5.28	6.4	12.2	80
CZ^R(58-42) + Co + Rh(0.5)	5.28	6.5	12.7	72
CZ^S(80-20)	5.36	5.0	–	68
CZ^S(80-20)Co	5.35	4.4	14.0	63
CZ^S(80-20)Co–Rh(0.5)	5.35	4.5	14.0	78
CZ^S(80-20)Co–Rh(1.0)	5.35	4.3	15.8	97
CZ^R(80-20)	5.34	7.3	–	84
CZ^R(80-20) + Co	5.34	7.3	11.5	80
CZ^R(80-20) + Co + Rh(0.5)	5.34	7.3	12.1	78
CZ^R(80-20) + Co + Rh(1.0)	5.34	7.3	11.2	79

through the full width at maximum half-height (FWMH) of the most intense and least overlapped peak.

$$a = d \cdot \sqrt{h^2 + k^2 + l^2} \quad (1)$$

The micro-homogeneity of the catalysts was studied by transmission electron microscopy (TEM) coupled to energy dispersive X-ray spectroscopy (EDX) analysis on a TOPCON EM-002B apparatus (acceleration voltage 200 kV).

The reducibility of mixed oxides was studied by temperature programmed reduction (TPR). The TPR measurements were carried out on a Micromeritics AutoChem II, with 100 mg of catalyst heated from room temperature to 1000 °C at 10 °C min^{-1} under 10% H_2 in Ar (50 mL min^{-1}). In order to evaluate precisely the hydrogen consumption, a TPD under argon was performed prior to TPR by heating the catalyst from room temperature to 500 °C. The hydrogen consumptions were measured using a thermal conductivity detector.

Co K-edge XANES (X-ray absorption near edge structure) spectra were obtained in transmission mode at room temperature on the SAMBA beam line at SOLEIL (Gif-sur-Yvette, France). A sagitally focusing double crystal Si(1 1 1) monochromator was used. The energy was scanned from 7502 to 8500 eV with incremental steps of 2 eV/point from 7502 to 7700 eV, 0.2 eV/point from 7700 to 7740 eV, 0.5 eV/point from 7740 to 7830 eV and 2 eV/point from 7830 to 8500 eV. The energy was calibrated to the first inflection point of a Co metal foil. A total of 2 scans were collected for each sample. XANES spectra were background corrected and normalized in the middle of the first EXAFS oscillation with the Athena package [22].

2.3. Catalytic reactivity tests

Reforming reaction was carried out under realistic internal combustion engine exhaust gas conditions in conventional quartz fixed bed reactor. Samples were loaded onto the center of the reactor between quartz wool. Tests were performed at 150,000 h^{-1}, under a 3 L h^{-1} gas flow composed of 12% CO_2 + 13.5% H_2O + 1% O_2 + 1.6% isooctane + inert gases (N_2 + Ar). The amount of co-fed hydrocarbon was adjusted to the aimed H_2 value of 10% determined by thermodynamics calculations [21]. The gas products were analyzed on-line by micro-gas chromatography. Hydrocarbons (C_2–C_5) were analysed on alumina column, methane and carbon dioxide on Poraplot column, isooctane and water on OV-1 column, hydrogen, oxygen, nitrogen, methane and carbon monoxide on molecular sieve (MS5A) column.

3. Results and discussion

3.1. Characterization

3.1.1. Textural and structural characterization

The specific surface areas of catalysts prepared via the pseudo sol–gel method range between 64 and 97 $m^2\,g^{-1}$ (Table 2), which are relatively high values for ceria–zirconia materials. Forasmuch as CZ^S(58-42) and CZ^S(80-20) BET areas are very close (64 and 68 $m^2\,g^{-1}$), the content in ceria has no incidence on the specific surface area, as previously noticed in the literature [23].

The specific surface areas of the impregnated catalysts reach values between 72 and 80 $m^2\,g^{-1}$. The specific surface areas of the supports supplied by Rhodia are higher than that of the supports prepared by sol–gel route, but after deposition of metals, the specific surface areas of the impregnated catalysts become similar to the corresponding sol–gel catalysts.

XRD patterns of stoichiometric ceria–zirconia based mixed oxides, presented in Fig. 2, exhibit peaks at 2θ = 29°, 33°, 48°, 57°, 60°, 71°, 78°, 80°, 90°, 98° which can be indexed to a face-centered cubic phase of ceria–zirconia ($Ce_{0.6}Zr_{0.4}O_2$, JCPDS no. 38-1439, space group: *Fm*3*m*). The fluorite structure observed for stoichiometric ceria–zirconia is even preserved when metallic cations are added during the preparation. A weak peak is detected at 36.8° and

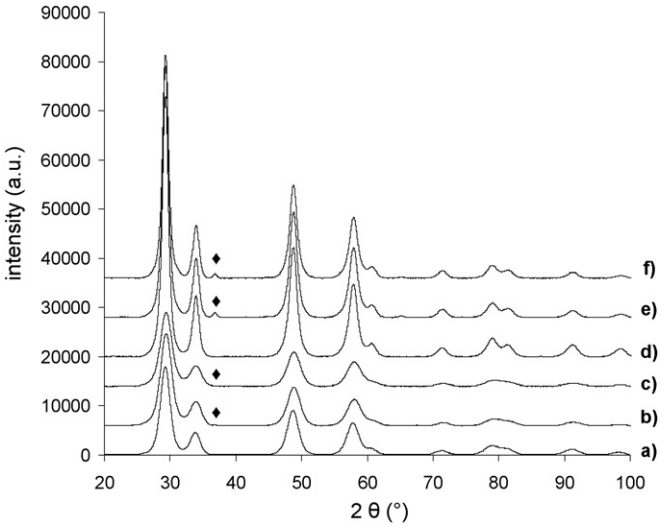

Fig. 2. XRD patterns of mixed oxides: (a) CZ^S(58-42), (b) CZ^S(58-42)Co, (c) CZ^S(58-42)Co–Rh(0.5), (d) CZ^R(58-42), (e) CZ^R(58-42) + Co, and (f) CZ^R(58-42) + Co + Rh(0.5), (◆) Co_3O_4 (3 1 1) peak.

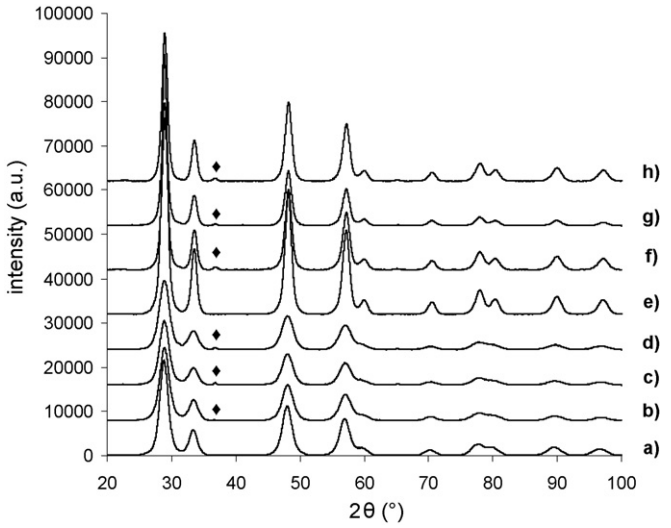

Fig. 3. XRD patterns of mixed oxides: (a) CZ^S(80-20), (b) CZ^S(80-20)Co, (c) CZ^S(80-20)Co–Rh(0.5), (d) CZ^S(80-20)Co–Rh(1.0), (e) CZ^R(80-20), (f) CZ^R(80-20) + Co, (g) CZ^R(80-20) + Co + Rh(0.5), and (h) CZ^R(80-20) + Co + Rh(1.0), (◆) Co_3O_4 (3 1 1) peak.

can be attributed to cobalt oxide cubic phase (Co_3O_4, JCPDS no. 43-1003). It is visible mostly for the impregnated catalysts and, for sol–gel catalysts, it may indicate that a fraction of cobalt oxide has been rejected from the ceria–zirconia structure. The low content of rhodium does not allow one to detect any crystalline phase associated to this metal.

XRD patterns of ceria-rich ceria–zirconia based mixed oxides, presented in Fig. 3, exhibit peaks at lower 2θ than stoichiometric ceria–zirconia based ones, due to the expansion of the unit cell with an increase of Ce content. These peaks can be indexed to a face-centered cubic phase of ceria–zirconia ($Ce_{0.75}Zr_{0.25}O_2$, JCPDS no. 28-0271, space group: *Fm*3*m*). The remarks drawn for stoichiometric systems about some cobalt oxide rejection also apply to ceria-rich catalysts. It is worth noting that for these catalysts, the peak at 36.8° corresponding to Co_3O_4 rejected from the mixed oxide of the sol–gel catalysts, is of higher intensity compared to the stoichiometric catalysts series.

Structural characteristics of both sol–gel and impregnated catalysts are detailed in Table 2. The cubic lattice parameter of sol–gel stoichiometric ceria–zirconia based catalysts exhibits a low variation compared to the pure mixed oxide (from 5.29 to 5.27 Å). This could reveal cobalt insertion which could decrease lattice parameter from 5.29 to 5.27 Å. The contraction of the unit cell may arise from the presence of the smaller 6-fold coordinated Co^{2+} ions (0.75 Å) in the matrix, compared to the larger structural cations (Ce^{4+}: 0.97 Å, Zr^{4+}: 0.84 Å) [24]. Rhodium co-insertion maintains this lattice parameter to 5.27 Å, since the 6-fold coordinated Rh^{3+} ions have an ionic radius of 0.67 Å, close to the one of the Co^{2+} ions. For impregnated catalysts, the lattice parameter is unchanged (5.28 Å) when metals are added, indicating that no metal insertion occurs.

The cubic lattice parameter of ceria-rich catalysts is higher than that of the stoichiometric ceria–zirconia based catalysts (5.34–5.36 Å compared to 5.29 Å). The unit cell of the mixed oxide expands with the increase of ceria content in mixed oxides, according to Vegard's law, because of the larger ionic radius of 8-fold coordinated Ce^{4+} ion (0.97 Å) compared with Zr^{4+} (0.84 Å) [24,25]. As mentioned above, cobalt insertion could lead to a slight decrease of the lattice parameter for sol–gel catalysts (5.35 Å) whereas it is maintained at 5.34 Å for impregnated catalysts.

Particle sizes of mixed oxides belong to the nanoparticles range (3.8–5.0 nm for sol–gel catalysts calcined at 500 °C and 6.4–7.3 for catalysts prepared by impregnation on supports prepared by a calcination at a temperature higher than 500 °C). The particle size of cobalt oxide are much larger (5.0–15.8 nm), revealing sintering of oxide cobalt particles. It's worth noting again, comparing the CZ^S(58-42) to the CZ^S(80-20) series, the increase of size of Co_3O_4 particles rejected from the mixed oxides prepared by sol–gel route.

3.1.2. Transmission electron microscopy

Two characteristic catalysts have been studied by TEM and their micro-homogeneity has been controlled by EDXS micro-analysis.

For CZ^S(58-42)Co–Rh(0.5) catalyst (Table 3), the local analyses are close to the global and theoretical values expected for Ce, Zr, Co, evidencing the good homogeneity of the mixed oxide. This confirms that the large Co_3O_4 particles detected by XRD are scarce. The low content of Rh avoids its detection; one can suppose that it is well dispersed in the catalyst.

For CZ^R(58-42) + Co + Rh(0.5) catalyst (Table 3), prepared by impregnation, local measurements globally correspond to the theoretical expected values but some heterogeneities exist in the cobalt and rhodium distributions. This can be linked to the clear detection of Co_3O_4 particles by XRD.

3.1.3. X-ray absorption spectroscopy

As X-ray diffraction evidenced partial insertion and partial rejection of cobalt for the sol–gel catalysts, further investigation was carried out on these materials, in order to clarify cobalt speciation in the mixed oxides. Therefore, Co K-edge XANES spectra were examined in order to determine the speciation of

Table 3
EDX analyses of CZ^S(58-42)Co–Rh(0.5) and CZ^R(58-42) + Co + Rh(0.5) catalysts.

Catalyst code	Analysis	Composition (wt.%)			
		Ce	Zr	Co	Rh
CZ^S(58-42)Co–Rh(0.5)	Theoretical value	56.4	36.7	6.2	0.7
	Global analysis	57.0	37.1	5.9	0.0
	Local analysis - 1	71.2	25.9	2.8	0.0
	Local analysis - 2	60.1	35.3	4.7	0.0
	Local analysis - 3	62.6	32.0	5.5	0.0
	Local analysis - 4	55.5	39.6	4.9	0.0
	Local analysis - 5	64.2	26.4	9.4	0.0
	Local analysis - 6	57.5	38.7	3.8	0.0
	Local analysis - 7	57.5	36.4	6.2	0.0
CZ^R(58-42) + Co + Rh(0.5)	Theoretical value	56.4	36.7	6.2	0.7
	Global analysis	57.4	35.5	5.5	1.6
	Local analysis - 1	56.2	34.1	7.7	1.9
	Local analysis - 2	53.7	36.2	10.2	0.0
	Local analysis - 3	61.2	34.6	4.2	0.0
	Local analysis - 4	59.2	38.3	2.5	0.0

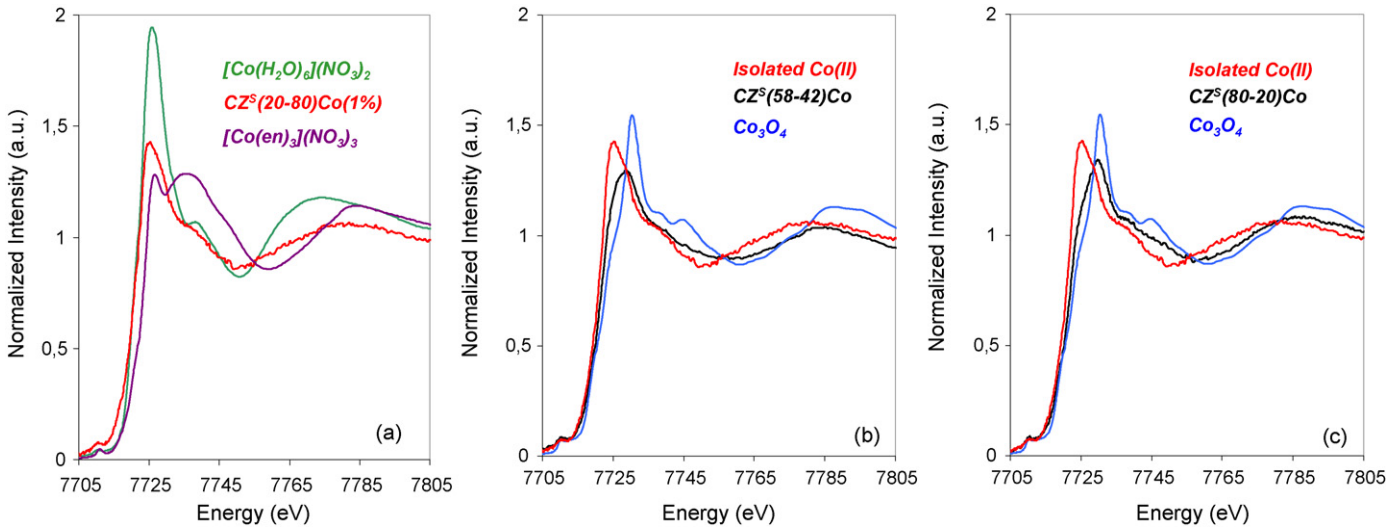

Fig. 4. XANES Co K-edge spectra of mixed oxides: (a) CZ^S(20-80)Co(1%) compared to reference compounds of Co(II) and Co(III), (b) CZ^S(58-42)Co, and (c) CZ^S(80-20)Co, compared to spectra of isolated Co(II) and Co_3O_4 spectra.

cobalt in CZ^S(58-42)Co and CZ^S(80-20)Co and its insertion in or rejection from the mixed oxide structure depending on the CeO_2/ZrO_2 ratio. X-ray absorption spectroscopy in the XANES region is a powerful method to identify the oxidation state of the supported species, discriminate between isolated species and cobalt oxide, and evaluate the proportion of cobalt oxide [26–28].

A reference sample was prepared using a zirconia-rich ceria–zircona matrix (20–80%) with a Co loading of 1 wt.% (i.e., 5 times less than the catalysts described above). The composition was chosen so as to limit Co rejection. The XANES spectrum of this sample is compared with those of two reference salts: $[Co(II)(H_2O)_6](NO_3)_2$ corresponding to octahedral Co(II) ions and $[Co(III)(en)_3](NO_3)_3$ corresponding to octahedral Co(III) ions (Fig. 4(a)). The edge position for CZ^S(20-80)Co(1.0) is identical to that of Co(II) nitrate (7726 eV), which confirms that cobalt is present as Co^{2+} ions in the matrix. This sample will be used as typical for Co^{2+} ions inserted in a ceria–zirconia matrix, as opposed to rejected oxide particles of Co_3O_4.

Fig. 4(b) and (c) exhibit XANES spectra recorded on CZ^S(58-42)Co and CZ^S(80-20)Co, compared to the spectra of CZ^S(20-80)Co(1.0) and Co_3O_4. The presence of isosbestic points below 7765 eV (at about 7728.8 and 7757.0 eV) tends to show that the Co monometallic catalysts can be treated in a first approximation as a mixture between Co^{2+} ions in the ceria–zirconia matrix and Co_3O_4 particles, which is in line with XRD results. The absence of isobestic points for the first EXAFS oscillation can arise from different distances between Co and its neighbours depending on the ceria content, resulting in a shift of the oscillation position. The white line measured on the Co monometallic catalysts is asymmetric, with a shoulder at lower energy corresponding to Co^{2+} ions, and a peak at higher energy corresponding to Co_3O_4, which is clearly seen in Fig. 4(c). The contribution of the low energy shoulder

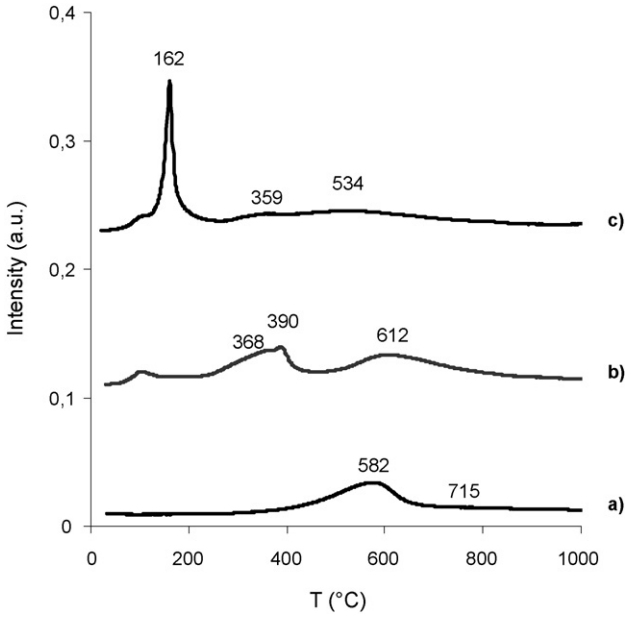

Fig. 5. TPR profiles of stoichiometric ceria–zirconia based mixed oxides prepared by sol–gel: (a) CZ^S(58-42), (b) CZ^S(58-42)Co, and (c) CZ^S(58-42)Co–Rh(0.5).

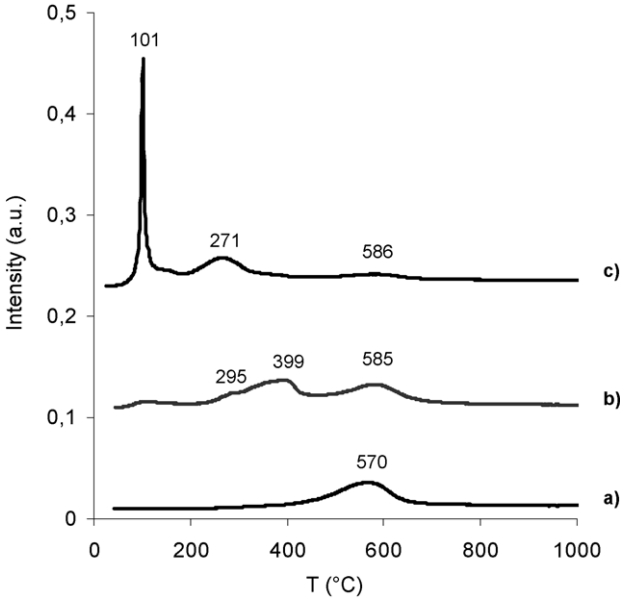

Fig. 6. TPR profiles of stoichiometric ceria–zirconia based mixed oxides prepared by impregnation: (a) CZ^R(58-42), (b) CZ^R(58-42) + Co, and (c) CZ^R(58-42) + Co + Rh(0.5).

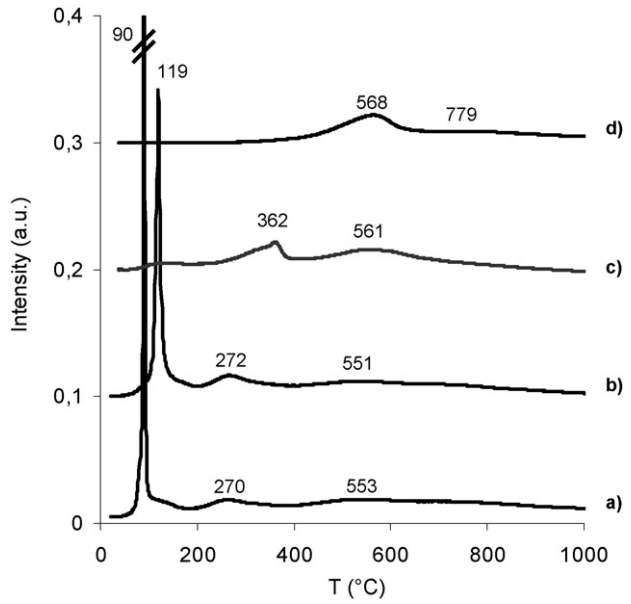

Fig. 7. TPR profiles of ceria-rich ceria–zirconia based mixed oxides prepared by sol–gel: (a) CZ^S(80-20)Co–Rh(1.0), (b) CZ^S(80-20)Co–Rh(0.5), (c) CZ^S(80-20)Co, and (d) CZ^S(80-20).

decreases from CZ^S(58-42)Co to CZ^S(80-20)Co, while the position of the main peak shifts to a higher energy (from 7728.8 to 7730.1 eV), confirming a higher rejection of cobalt toward oxide particles when the ceria content increases in the matrix. This confirms XRD observations about the intensity of Co_3O_4 peak and the particle size of cobalt oxide both increasing with the ceria content.

3.1.4. Temperature programmed reduction

TPR profiles of stoichiometric ceria–zirconia based catalysts prepared by sol–gel method are presented in Fig. 5. Sol–gel stoichiometric ceria–zirconia exhibits one main reduction peak at 582 °C and a shoulder at 715 °C (Fig. 5(a)), corresponding respectively to surface and bulk ceria reduction [29]. Insertion

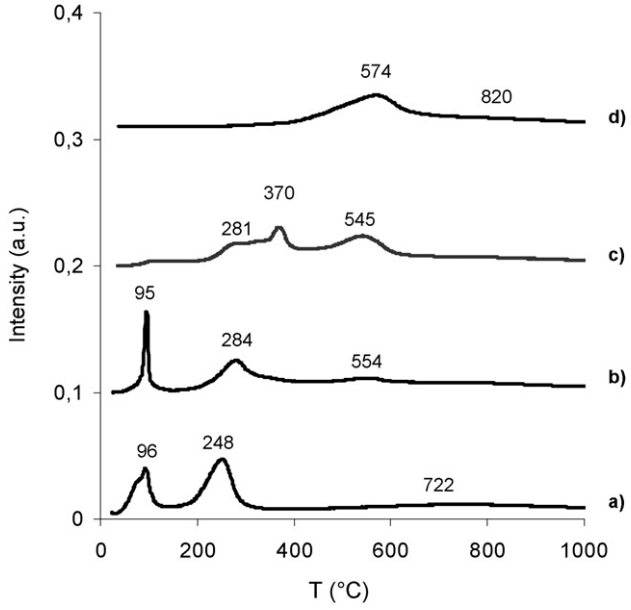

Fig. 8. TPR profiles of ceria-rich ceria–zirconia based mixed oxides prepared by impregnation: (a) CZ^R(80-20) + Co + Rh(1.0), (b) CZ^R(80-20) + Co + Rh(0.5), (c) CZ^R(80-20) + Co, and (d) CZ^R(80-20).

Table 4
Reducibility of prepared catalysts.

Catalyst code	Total H_2 consumption (mmol g^{-1})	Theoretical H_2 consumption for metals (mmol g^{-1})	Reducibility of ceria (%)
CZ^S(58-42)	1.50	–	90.0
CZ^S(58-42)Co	2.95	0.99	127.8
CZ^S(58-42)Co–Rh(0.5)	2.99	0.96	135.9
CZ^R(58-42)	1.43	–	84.2
CZ^R(58-42) + Co	2.39	1.15	79.4
CZ^R(58-42) + Co + Rh(0.5)	2.90	1.16	111.9
CZ^S(80-20)	1.45	–	65.8
CZ^S(80-20)Co	2.40	0.94	70.8
CZ^S(80-20)Co–Rh(0.5)	2.83	1.00	88.2
CZ^S(80-20)Co–Rh(1.0)	3.03	0.98	99.6
CZ^R(80-20)	1.69	–	72.7
CZ^R(80-20) + Co	2.52	1.09	66.5
CZ^R(80-20) + Co + Rh(0.5)	2.18	1.16	47.9
CZ^R(80-20) + Co + Rh(1.0)	2.20	1.16	49.0

of cobalt in the mixed oxide results in a decrease of these temperatures, at it has been previously evidenced at the laboratory [19,30], since peaks are detected at 368 and 390 °C, both corresponding to cobalt and ceria surface reduction, and 612 °C which could correspond to ceria bulk reduction assisted by the presence of cobalt (Fig. 5(b)). However, surface area of this signal is much more important than the surface area of bulk ceria reduction peak of CZ^S(58-42) (Fig. 5(a) compared to Fig. 5(b)). Another interpretation is that this signal corresponds to reduction of cobalt inserted inside the structure, peaks at 368 and 390 °C corresponding to reduction of free Co_3O_4 into CoO then into Co metal and reduction of ceria surface. This would be in good agreement with what obtained on similar Ni-based systems [31].

Rhodium insertion shifts the main reduction peak at a much lower temperature, 162 °C (Fig. 5(c)), in accordance with literature for reduction of Rh^{3+} to Rh^0 at such a temperature [32], and favours reduction of the other species at lower temperature.

TPR profiles of stoichiometric ceria–zirconia based catalysts prepared by impregnation method are presented in Fig. 6. Commercial stoichiometric ceria–zirconia exhibits one main reduction peak at 570 °C (Fig. 6(a)), the high temperature peak being probably too small to be detected. Cobalt oxide reduces between 300 and 400 °C (Fig. 6(b)). Rhodium, deposited on the surface reduces at a low temperature of 101 °C (Fig. 6(c)),

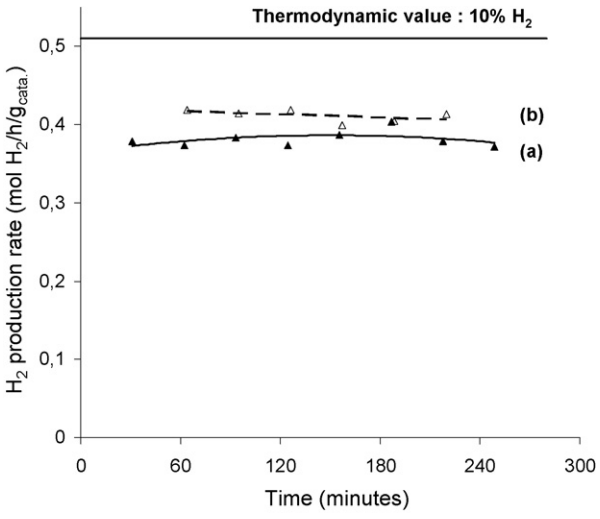

Fig. 9. H_2 production rate during reactivity tests with stoichiometric ceria–zirconia based bimetallic catalysts: (a) CZ^S(58-42)Co–Rh(0.5) and (b) CZ^R(58-42) + Co + Rh(0.5).

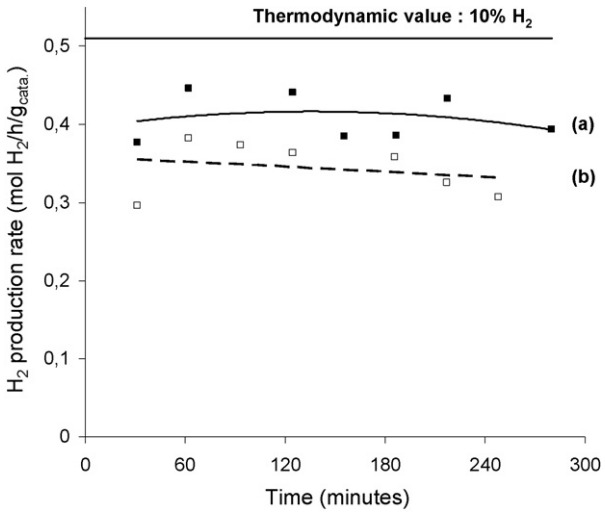

Fig. 10. H_2 production rate during reactivity tests with ceria-rich ceria–zirconia based bimetallic catalysts: (a) CZ^S(80-20) + Co + Rh(0.5) and (b) CZ^R(80-20)Co–Rh(0.5).

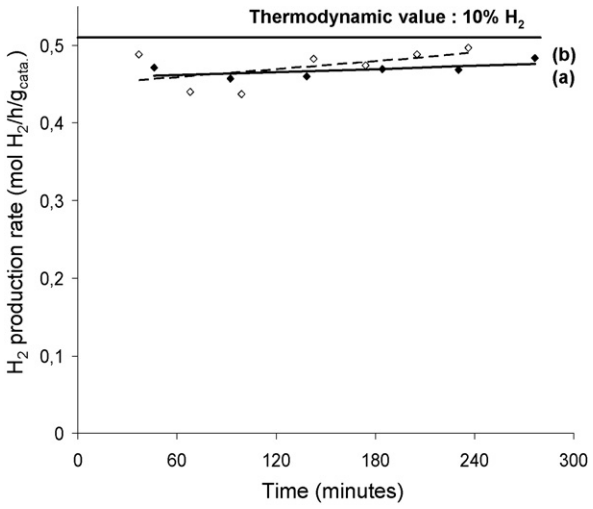

Fig. 11. H_2 production rate during reactivity tests with 1% Rh doped ceria–zirconia based bimetallic catalysts: (a) CZ^S(80-20)Co–Rh(1.0) and (b) CZ^R(80-20) + Co + Rh(1.0).

compared to 162 °C for CZ^S(58-42)Co–Rh(0.5). This is also an indication that Rh is on the surface and in poor interaction with the support, as for Co_3O_4 whose reduction occurs at 271 °C compared to 359 °C in the sol–gel material. It is also noticed that higher reduction temperature peak (570, 585, or 586 °C) is not modified by the impregnation of the metals and corresponds here to ceria reduction.

TPR profiles of ceria-rich ceria–zirconia based catalysts prepared by sol–gel method are presented in Fig. 7. Sol–gel ceria-rich ceria–zirconia exhibits two reduction peaks at 568 and 779 °C (Fig. 7(d)). The same observations about cobalt or rhodium effect on the temperature of reduction can be drawn. Here too, cobalt addition diminishes reduction temperature of ceria and rhodium addition the reduction temperature of cobalt oxide. Doping with 1% Rh enhances the reducibility of the mixed oxide, which begins to reduce at a very low temperature (90 °C) with rhodium (Fig. 7(a)).

TPR profiles of ceria-rich ceria–zirconia based catalysts prepared by impregnation method are presented in Fig. 8. Pure ceria-rich ceria–zirconia exhibits two reduction peaks at 574 and 820 °C (Fig. 8(d)). Cobalt oxide deposited on the surface reduces between 281 and 370 °C. Rhodium reduces at a low temperature of 95–96 °C.

Cobalt and rhodium deposition has only a little effect on temperature of reducibility of ceria since it lowers it from 574 to 545 °C or 554 °C, respectively. Rhodium consumes hydrogen for

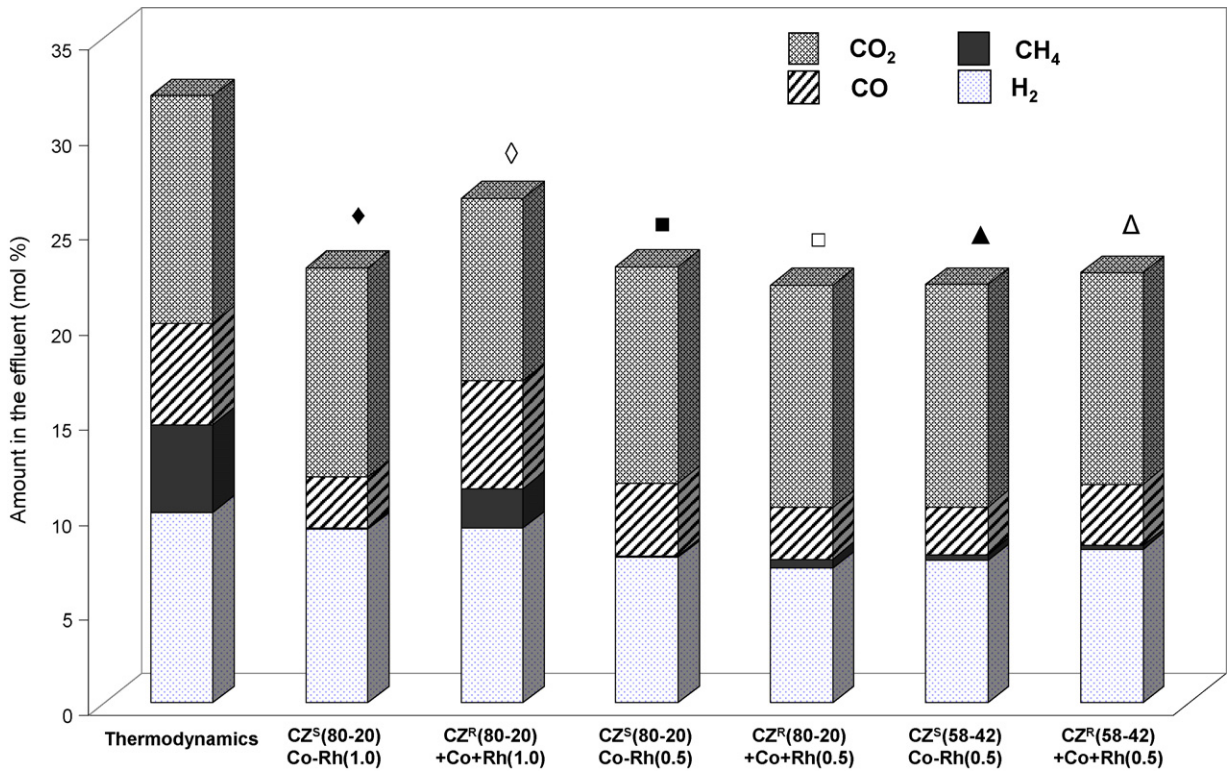

Fig. 12. Amount in the effluent (mol%) during reactivity tests with ceria–zirconia based bimetallic catalysts, compared to thermodynamic prediction.

Table 5
Hydrocarbons distribution.

Catalyst code	Methane (mol%)	Isobutane ($\times 10^{-3}$ mol%)	Isobutene ($\times 10^{-3}$ mol%)	$IsoC_4$ hydrocarbons ($\times 10^{-3}$ mol%)
CZ^S(80-20)Co–Rh(1.0)	0.10	1.1	16.3	17.4
CZ^R(80-20) + Co + Rh(1.0)	2.10	0.3	0.2	0.5
CZ^S(80-20)Co–Rh(0.5)	0.09	0.9	13.1	14.0
CZ^R(80-20) + Co + Rh(0.5)	0.50	0.2	3.2	3.4
CZ^S(58-42)Co–Rh(0.5)	0.32	0.3	2.0	2.3
CZ^R(58-42) + Co + Rh(0.5)	0.21	0.3	1.8	2.1

its reduction at low temperature (95 or 96 °C) but ceria is reduced at higher temperatures of 554 and 248 °C (Fig. 8(a) and (b)).

Reducibility of ceria has been calculated from hydrogen consumption, assuming that metallic cations of Co and Rh are totally reduced to metallic state, the remainder amount of hydrogen is consumed for ceria reduction (Table 4).

Noteworthy, for stoichiometric mixed oxides, introduction of metals improves ceria reducibility, disregarding the overestimated H_2 consumption probably due to carbonate decomposition at high temperature which modify TCD signal, since it increases with cobalt insertion from 90 to 127.8% and to 135.9% with Rh doping. On the other hand, cobalt impregnation has no effect on the extent of reducibility of ceria (which is quite similar to the pure mixed oxide, 84.2 and 79.4%), whereas rhodium impregnation enhances it to a lesser degree than for sol–gel corresponding catalyst (about 112% compared to 136%), due to spillover process [33].

For sol–gel ceria-rich catalysts, insertion of cobalt enhances ceria reducibility from 65.8 to 70.8%. Doping with Rh enhances far more this reducibility to 88.2 and 99.6%. On the contrary, impregnation of cobalt diminishes the reducibility of ceria from 72.7 to 66.5%, and rhodium addition decreases again this reducibility to 47.9 and 49.0%.

It could be remarked that the ceria reducibility is always higher for sol–gel mixed oxides compared to impregnated catalysts. One of the possible hypotheses is that the integration of metallic cation inside the structure enhances the oxygen mobility of this structure by modifying the cell parameter then favouring the reducibility of ceria.

3.2. Reactivity tests

In accordance with thermodynamics calculations [21], catalytic tests were performed at 520 °C with 1.6 mol% co-added isooctane with the objective to produce after reaction an effluent containing 10% of hydrogen.

All the catalysts prepared exhibit high activity, leading to a hydrogen production close to that associated with the thermodynamic equilibrium, under operating conditions based on realistic transposition of on-board application. However some variations in the catalytic behaviour can be discussed.

Stoichiometric bimetallic catalyst prepared by impregnation method exhibit a higher activity than the corresponding sol–gel catalyst (Fig. 9(b) compared to Fig. 9(a)). Ceria-rich bimetallic catalyst with 0.5% Rh prepared by sol–gel method (Fig. 10(a)) shows a higher activity than impregnated corresponding catalyst (Fig. 10(b)). Increasing Rh loading to 1.0% leads to improve catalytic activity since these catalysts are close to thermodynamic value whatever is the preparation method (Fig. 11(a) and (b)), thus hardly possible to discriminate.

Comparing ceria-rich catalysts to stoichiometric ceria–zirconia based ones prepared by sol–gel method, it is worth noting an enhancement of activity for higher ceria/zirconia ratio. This improvement of activity is possibly due to higher OSC of ceria-rich based mixed oxides compared to stoichiometric ceria–zirconia based ones [23,34].

The amounts of the main products in the effluent after catalytic reactions are presented in Fig. 12, the detailed distributions among hydrocarbons are given in Table 5.

CO_2 is always produced in a major amount with respect to CO, accordingly to the prediction of thermodynamics. The production of CH_4 is always much lower than expected from thermodynamics. $IsoC_4$ (isobutene and isobutane, in a lesser extent) are always detected in the gas phase, in different amounts depending on the preparation method of the catalysts. From Table 5, it appears that CH_4 and $isoC_4$ production always vary in the opposite way. For the ceria-rich catalysts, the percentage of methane is always higher for the impregnated catalysts than for the corresponding sol–gel catalysts, whereas the amount of $isoC_4$ is always high for the sol–gel systems. Although the formation of isobutene is never discussed in the literature of isooctane reforming, it can be thought as the primary product of isooctane activation by β-scission and could then be favoured, as a redox process (oxidative catalytic cracking), by catalysts with high oxygen mobility, whereas further C–C bond breaking would take place on metallic sites (α-scission).

4. Conclusions

Stoichiometric and ceria-rich ceria–zirconia based catalysts have been prepared by sol–gel route and impregnation method. Precursor method used for sol–gel catalysts synthesis allows partial integration of metallic cations as evidenced by XRD and Co K-edge XANES experiments. Insertion of octahedral Co^{2+} in the lattice modifies the physicochemical properties of the ceria–zirconia, improving reducibility of the mixed oxides. The cobalt insertion is disfavoured by high ceria content.

All the catalysts present high activity in hydrogen production by isooctane reforming, able to satisfy the requirements for on-board application in EGR. The integration of cobalt in the fluorite lattice prevents its loss from the catalyst to the exhaust.

At similar hydrogen production, the catalysts prepared from sol–gel method, modified by partial cobalt integration in the ceria–zirconia lattice, favour β-scission of isooctane into $isoC_4$, present at the trace level, whereas impregnated catalysts exhibit a much stronger metallic behaviour and favour CH_4 as by-product.

Acknowledgements

The authors acknowledge SOLEIL for provision of synchrotron radiation facilities and would like to thank staff for assistance in using beam line SAMBA. This work has been financially supported by the ADEME, via ANR-PREDIT RECONOME.

References

[1] G. Djéga-Mariadassou, F. Fajardie, J.-F. Tempère, J.-M. Manoli, O. Touret, G. Blanchard, J. Mol. Catal. A 161 (2000) 179–189.
[2] R. Burch, J.P. Breen, F.C. Meunier, Appl. Catal. B 39 (2002) 283–303.
[3] A.C. Gluhoi, S.D. Lin, B.E. Nieuwenhuys, Catal. Today 90 (2004) 175–181.
[4] L. Olsson, E. Fridell, J. Catal. 210 (2002) 340–353.
[5] M. Zheng, G.T. Reader, J.G. Hawley, Energy Convers. Manage. 45 (2004) 883–900.
[6] G.H Abd-Alla, Energy Convers. Manage. 43 (2002) 1027–1042.
[7] R.S.G. Baert, D.E. Beckman, A. Veen, SAE Paper 1999-01-0837.

[8] N. Ladommatos, S. Abdelhalim, H. Zhao, Appl. Therm. Eng. 18 (1998) 963–980.
[9] G. Stumpp, W. Banzhaf, SAE Paper 1978-780222.
[10] J.B. Heywood, International Combustion Engine Fundamentals, MGraw-Hill, New York, 1998.
[11] A. Maiboom, X. Tauzia, J.-F. Hétet, Energy 33 (2008) 22–34.
[12] S.L. Lee, T. Ahmad, J.P. Myers, SAE Technical Paper Series, 1981-811195.
[13] J.C. Summers, S. Van Houtte, D. Psaras, Appl. Catal. B 10 (1996) 139–156.
[14] J. Schäfer, M. Sommer, S. Diezinger, D. Trimis, F. Durst, J. Power Sources 154 (2006) 428–436.
[15] Y. Jamal, M.L. Wyszynski, Int. J. Hydrogen Energy 19 (1994) 557–572.
[16] A. Tsolakis, A. Megaritis, M.L. Wyszynski, Energy Fuels 17 (2003) 1464–1473.
[17] Y. Jamal, T. Wagner, M.L. Wyszynski, Int. J. Hydrogen Energy 21 (1996) 507–519.
[18] S.L. Swartz, P.H. Matter, G.B. Arkenberg, F.H. Holcomb, N.M. Josefik, J. Power Sources 188 (2009) 515–520.
[19] J.C. Vargas, S. Libs, A.C. Roger, A. Kiennemann, Catal. Today 107–108 (2005) 417–425.
[20] G. Blanchard, A.C. Roger, A. Kiennemann, E. Ambroise, C. Courson, Catalyseur pour le vaporéformage d'hydrocarbures à base de Rhodium ou de Ruthénium sur des supports à base de Cérium et de Zirconium, patent request deposited on February 11, 2009.
[21] E. Ambroise, C. Courson, A. Kiennemann, A.C. Roger, O. Pajot, E. Samson, G. Blanchard, Top. Catal. 52 (2009) 2101–2107.
[22] B. Ravel, M. Newville, J. Synchrotron Rad. 12 (2005) 537–541.
[23] S. Rossignol, Y. Madier, D. Duprez, Catal. Today 50 (1999) 261–270.
[24] R.D. Shannon, Acta Crystallogr. Sect. A 32 (1976) 751.
[25] S. Meriani, Mater. Sci. Eng. A 109 (1989) 121–130.
[26] M. Mhamdi, E. Marceau, S. Khaddar-Zine, A. Ghorbel, M. Che, Y. Ben Taarit, F. Villain, Z. Phys. Chem. 219 (2005) 963–978.
[27] H. Ben Boubaker, M. Mhamdi, E. Marceau, S. Khaddar-Zine, A. Ghorbel, M. Che, Y. Ben Taarit, F. Villain, Micropor. Mesopor. Mater. 93 (2006) 62–70.
[28] F. Dumond, E. Marceau, M. Che, J. Phys. Chem. C 111 (2007) 4780–4789.
[29] M.F.L. Johnson, J. Mooi, J. Catal. 103 (1987) 502–505.
[30] M. Virginie, M. Araque, A.C. Roger, J.C. Vargas, A. Kiennemann, Catal. Today 138 (2008) 21–27.
[31] F. Ocampo, B. Louis, A.C. Roger, Appl. Catal. A: Gen. 369 (2009) 90–96.
[32] C. Diagne, H. Idriss, A. Kiennemann, Catal. Commun. 3 (2002) 565–571.
[33] S. Bernal, J.J. Calving, G.A. Cifredo, J.M. Rodríguez, V. Perrichon, A. Laachir, J. Catal. 137 (1992) 1–11.
[34] P. Fornasiero, R. Di Monte, G. Ranga Rao, J. Kašpar, S. Meriani, A. Trovarelli, M. Graziani, J. Catal. 151 (1995) 168.